21st Australasian Fluid Mechanics Conference
Adelaide, Australia
10-13 December 2018

Can Difference in Pulsatile Waveform Change Patient's Outcomes?

E.K.W. Poon[1], V. Thondapu[1,2], P. Barlis[1,2] and A.S.H. Ooi[1]

[1]Department of Mechanical Engineering, Melbourne School of Engineering
The University of Melbourne, Victoria 3010, Australia

[2]Melbourne Medical School, Faculty of Medicine, Dentistry & Health Science
The University of Melbourne, Victoria 3010, Australia

Abstract

In this study, we aim to identify the importance in employing an individualised pulsatile waveform on the prediction of future clinical events after stent deployment. By systematically analysing the micro-recirculation developments of a stented coronary artery under different pulses, it is demonstrated that micro-recirculation environments enlarge in size at systole and diminish as flow accelerates towards peak flow at diastole. However, the size of these recirculation environments is very sensitive to the characteristics of each individual pulsatile waveform even though both pulses have identical time-averaged flow rate. The differences are most pronounced at systole for both apposed and malapposed stent configurations, but discrepancy can also be observed at late diastole in a malapposed strut. The present investigation has contributed to better fundamental knowledge in post-stenting pulsatile haemodynamics, and hence improvements in personalised stent development and/or deployment strategies.

Introduction

The human cardiovascular system is a sophisticated flow network with complicated haemodynamic environments. At the core of the cardiovascular system, our heart periodically supplies blood to maintain functionalities of our bodies. These periodic blood flow movements change from time to time, and from person to person. Yet despite increasing awareness on the effects of pulsating flow environments (especially the macro [1] and micro-recirculations [2] in the coronaries), typical computational fluid dynamics (CFD) modelling of haemodynamics in the cardiovascular system often relies on population-specific pulsatile waveform rather than direct patient-specific flow measurement [3-6].

In this study, we investigate the impacts of different pulsatile waveforms of the left coronary arteries on micro-recirculations development in the vicinity of the scaffolded coronary arterial segment based on co-workers' recent findings in [4,5]. Pulsatile, non-Newtonian CFD analyses are performed on a two-dimensional idealised stent strut. Under the effect of different pulsatile coronary flows, micro-recirculation environments are carefully analysed. These fundamental CFD studies will shed light on the importance of personalised pulsatile CFD simulations, and ultimately lead to more precise medical treatments/devices.

Methods

Two-Dimensional Stent Strut Geometry

Figure 1 shows the two-dimensional stent strut geometries considered in this study. The stent strut has a square cross-section and is 150 µm thick. Three strut configurations are chosen [7]. These cover both an apposed stent strut and intermediate malapposed stent struts that are commonly observed in intracoronary optical coherence tomography imaging data [7].

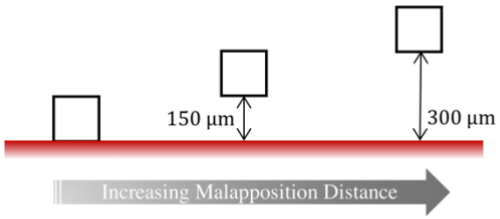

Figure 1. Schematic diagram showing the 2-dimensional stent strut configurations. On the left, the strut is apposed (touching) the arterial surface; Two additional strut malapposition distances are considered which are 150 and 300 μm from the arterial surface.

Computational Fluid Dynamics

Pulsatile blood flow through the coronary artery model is numerically simulated by directly solving the incompressible Navier–Stokes equations:

$$\frac{\partial \boldsymbol{u}}{\partial t} + \boldsymbol{u} \cdot \nabla \boldsymbol{u} = -\frac{\nabla P}{\rho} + \nabla \cdot \left(\frac{\mu}{\rho} (\nabla \boldsymbol{u} + \nabla \boldsymbol{u}^T) \right) \quad (1)$$

$$\nabla \cdot \boldsymbol{u} = 0 \quad (2)$$

where ρ = 1060 kg/m^3 is the constant blood density and the apparent viscosity, μ, of human blood is approximated using the Quemada model [8]. Equations (1) and (2) are discretized into finite-volume formulations using an in-house modified OpenFOAM-2.1.1 (OpenCFD Ltd., ESI group, Bracknell, UK) package. Details of the numerical method, including validation, can be found in [4].

Two physiological waveforms, Pulse 1 and Pulse 2 hereinafter refer as P1 and P2, from the left anterior descending artery are prescribed as the inflow boundary condition and results are

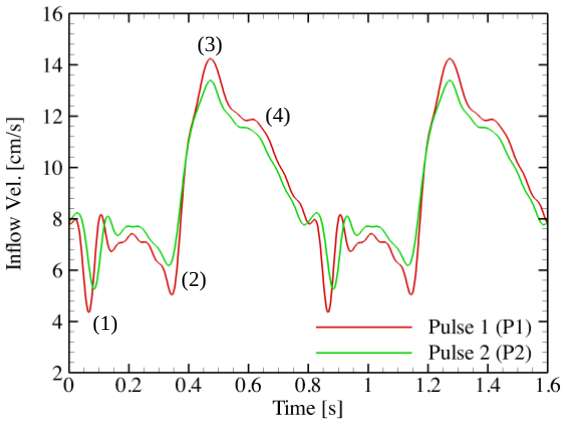

Figure 2. Pulsatile waveforms from the left anterior descending. Pulse 1 (P1) and Pulse 2 (P2). (1) systole, (2) early diastole, (3) peak flow and (4) late diastole.

analysed at 4 major time points during a cardiac cycle: (1) systole, (2) early diastole, (3) peak flow and (4) late diastole (see figure 2) [9,10]. The two waveforms are decomposed into 16 Fourier coefficients and artificially adjusted such that both have a mean flow rate of 39 mL/min. Similarly, both waveforms have a frequency of 75 beat per minute. No-slip boundary conditions are used at both rigid arterial wall and stent strut, whereas a zero pressure is employed at the outlet.

Results

Instantaneous Streamlines Pattern

Figures 3 and 4 demonstrate the evolution of the micro-recirculations for both the apposed stent strut and malapposed stent strut with malapposition distance (MD) = 150 μm under the two different pulses considered. The difference between the micro-recirculating environments of a malapposed stent strut with MD = 300 μm for the two pulses is somewhat similar to the cases demonstrated in figures 3 and 4 and hence is not presented.

In an apposed stent strut, micro-recirculations are formed both proximal and distal to the strut. For pulse 1 (P1), micro-recirculations are most pronounced during systole (low coronary flow, first panel). In fact, the two micro-recirculations almost join together to form a large region of flow reversal enveloping the stent strut. Micro-recirculations are almost suppressed at early diastole (rapid increase in coronary flow; second panel). However, they enlarge in size again at peak

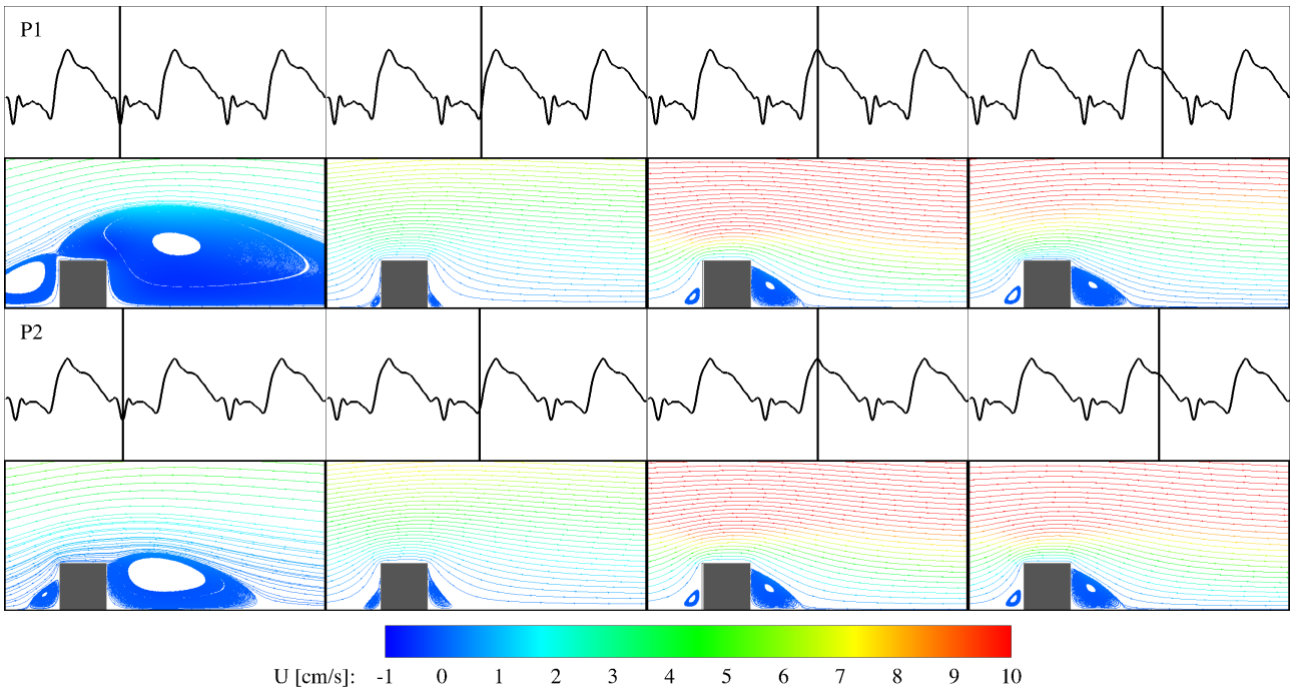

Figure 3. Instantaneous 2-dimensional streamlines showing the evolution of the micro-recirculations in the vicinity of an apposed stent strut at 4 important time points over a cardiac cycle. From left to right: systole; early diastole; peak flow and late diastole. (Top) Pulse 1 and (Bottom) Pulse 2.

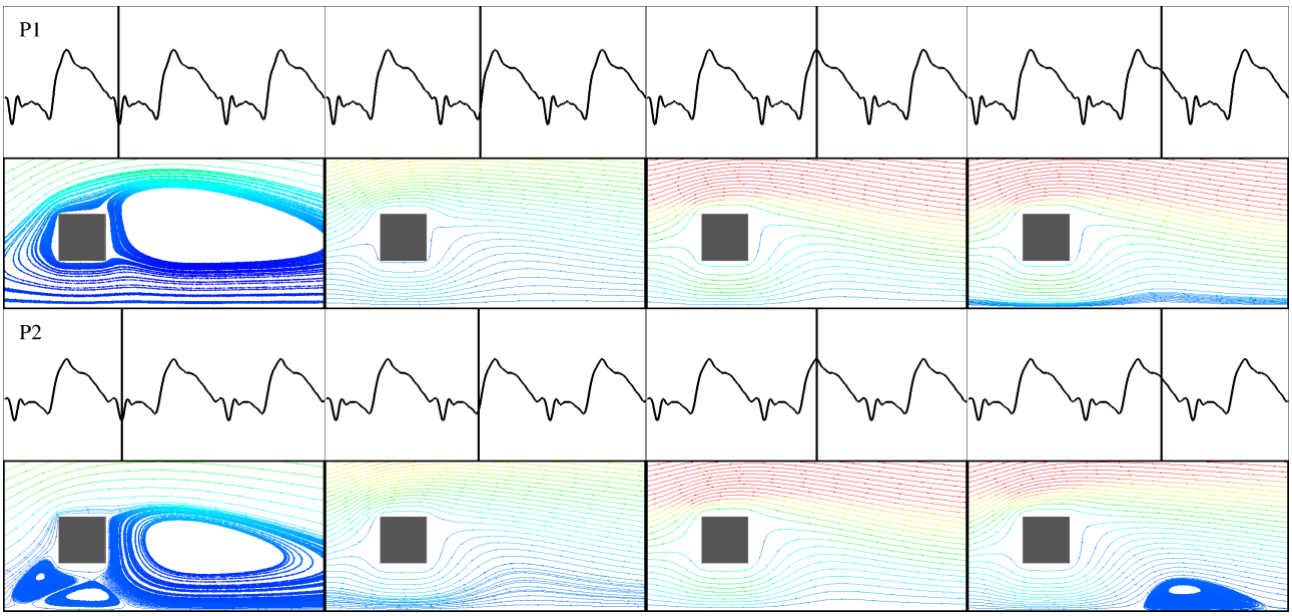

Figure 4. Instantaneous 2-dimensional streamlines showing the evolution of the micro-recirculations near a 150 μm malapposed stent strut at 4 important time points over a cardiac cycle. From left to right: systole; early diastole; peak flow and late diastole. Velocity contour levels are same in figure 3.

diastole (peak flow) and remain almost identical for the rest of the cardiac cycle.

The micro-recirculation environments of an apposed strut for pulse 2 (P2) almost follow an identical pattern as P1 (see figure 3), except that there are notable differences in the size of the micro-recirculations at both systole and early diastole. At systole, the micro-recirculations formed in P2 are significantly smaller than P1. The recirculating environments remain confined to the proximal and distal side of the strut unlike those in P1. In contrast, the micro-recirculations are relatively larger in P2 than in P1 at early diastole. These recirculations are almost identical in size for both pulses at peak flow and late diastole.

Strut malapposition leads to completely different haemodynamics as the strut is subjected to higher blood flow velocity away from the arterial wall (see figure 4). For P1, micro-recirculation is again most pronounced during systole. Instead of individual micro-recirculations proximal and distal to the stent strut, a large flow reversal region is formed that completely encompasses the stented area and results in reversal of flow near the arterial wall and a single focus distal to the stent strut. Although blood flow is distributed by the malapposed strut causing vertical deflection of streamlines distally, no micro-recirculation is observed for the rest of the cardiac cycle.

More micro-recirculations are observed for a malapposed strut in P2. During systole, multiple micro-recirculations are obverse for the first time – one proximally, one distally and one centred between the bottom of the strut and the arterial wall. The recirculations are also more compact in size as compared to P1, with both proximal and centre micro-recirculations barely exceed 150 μm in height and distal micro-recirculation almost flush with the top of the strut. The haemodynamics in the vicinity of the malapposed strut becomes nearly identical for both P1 and P2 for the next two time points. However, differences are again observed at late diastole where a single detached micro-recirculating zone is found at approximately 1 strut thickness (~150 μm) from the malapposed strut in P2.

Endothelial Shear Stress

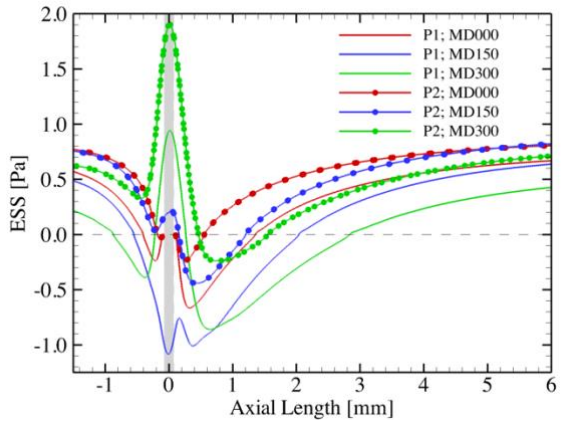

Figure 5. Endothelial shear stress (ESS) at systole. Grey colour box indicates the axial location of the stent strut. ESS on arterial surface is displayed and hence discontinued for apposed strut.

The effects of pulsatile waveforms on the endothelial shear stress (ESS) for both apposed and malapposed strut are individually analysed and presented in figure 5. Changes in ESS are compared at systole as the differences between micro-recirculations are most significant as demonstrated in figures 3 and 4. In general, the arterial surface is subjected to a higher value of ESS under P2 than P1. However, when considering atherogenic shear stress region (i.e. |ESS| < 0.5 Pa) [11], it is interesting to note that a malapposed stent strut with MD = 150 μm in P2 performed poorly in between the bottom of the strut and arterial surface (within grey box) as compared to the same strut configuration in P1. ESS for MD = 150 μm in P1 > 0.5 Pa and hence the endothelial cell linings are protected, maintaining essential vascular homeostasis.

Elevated Blood Viscosity

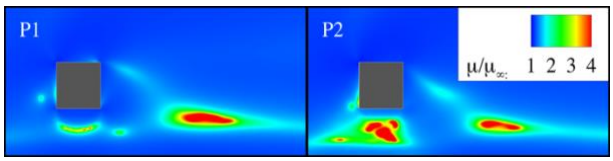

Figure 6. Contours of locally elevated blood viscosity relative to the infinitely shear thinning viscosity, μ_∞.

The clinical significance of the presence of multiple micro-recirculations in the vicinity of a 150 μm malapposed strut in P2 is also highlighted by the variations of local blood rheology as shown in figure 6. The elevation in viscosity ratio, μ/μ_∞, is employed to investigate not only the changes in blood viscosity near the lumen surface, but within the full computational domain. An elevated μ/μ_∞ value represents an increased in "stickiness" of blood. These high viscosity regions are clustered near the micro-recirculations and hence demonstrate a significant correlation between the two. Specifically, the high viscosity regions in between the bottom of the strut and arterial surface are substantially larger in P2 than in P1, which signify a higher chance of thrombogenic event in P2.

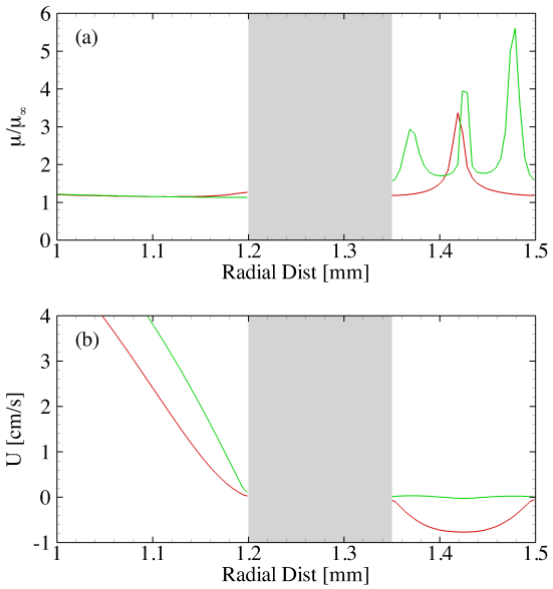

Figure 7. (a) Local elevation in blood viscosity and (b) local blood flow velocity along the centreline of the strut. Grey colour box indicates the radial location of the stent strut. P1 - Green line; P2 – Red line.

In fact, there are three instants where the local viscosity is elevated by more than 3-fold in between the bottom of the strut and arterial surface in P2 (see figure 7a). And the maximum local viscosity is almost double of that in P1. This combines with the nearly zero local velocity (refers to figure 7b) in between the bottom of the strut and arterial surface in P2 has therefore created a favourable environment for thrombosis formation. In contrast, the same may not be true for P1 as

relative high blood flow is observed at where local blood viscosity is elevated.

Discussions and Conclusion

In this study, CFD research tools are employed to better understand the changes in micro-recirculation environments under different pulsatile waveforms. Under the effect of pulsatile coronary flow, micro-recirculation environments are, in general, most pronounced at systole. The difference in these micro-recirculation environments between pulses is also most significant during systolic phase (see figures 3 and 4). In addition, the existence of these micro-recirculations depends strongly on the stent malapposition distance. In particular, one pulse may perform better than other in an apposed stent (figures 3), but poorly (with increasing number of micro-recirculations, suboptimal ESS, high local blood viscosity and low blood flow velocity) in a malapposed stent strut configuration (figures 4, 5, 6 and 7).

With the propensity to form abnormal thrombosis is commonly conceptualized through Virchow's triad [12], the presence of micro-recirculations represents stases in the blood stream and the attendant effect on local elevation in viscosity due to the formation of "Rouleaux" – stacks of red blood cells (RBCs). A similar effect was also reported in Ref. [4], wherein the large regions of high blood viscosity immediately distal to the malapposed stent signify the local accumulation of RBCs. It has been suggested such a condition may be a significant contributor to in-stent thrombosis [4,5], a highly complex and tightly regulated series of biochemical reactions involving RBCs, shear activated platelets, and coagulation factors interacting with dysfunctional endothelial cells and/or thrombogenic foreign bodies (struts).

Study Limitations

One of the major limitations is the lack of distensibility of the artery wall. The effects of cardiac systole on the coronary artery and the corresponding wave intensity on coronary haemodynamics are therefore unknown [13]. Another factor that might affect the present CFD analyses is the use of a developed velocity inlet boundary condition where turbulent intensity at the coronary ostia is not considered [14].

Acknowledgments

The authors would like to acknowledge the support of the Australian Research Council (LP150100233). This research was undertaken with the assistance of resources and services from the National Computational Infrastructure (NCI), which is supported by the Australian Government.

References

[1] Tenekecioglu, E., Poon, E.K.W., Carlos, C., Thondapu, V., Torii, R., Bourantas, C.V., Zeng, Y., Onuma, Y., Ooi, A.S.H., Serruys, P.W., and Barlis, P., The Nidus for Possible Thrombus Formation, *JACC Cardiovasc. Intervention*, **9**(20), 2016, 2167–2168.

[2] Barlis, P., Poon, E.K.W., Thondapu, V., Grundeken, M.J., Tu, S., Hayat, U., Ooi, A, Moore, S., Tenekecioglu, E., Wykrzykowska, J.J. & Serruys, P.W. Reversal of flow between serial bifurcation lesions: insights from computational fluid dynamic analysis in a population-based phantom model, *EuroIntervention*, **11**(5), 2015, e1-3.

[3] Chen, W.X., Poon, E.K.W., Thondapu, V., Hutchins, N., Barlis, P. & Ooi, A., Haemodynamic Effects of Incomplete Stent Apposition in Curved Coronary Arteries, *J. Biomech.*, **63**, 2017, 164–173.

[4] Poon, E.K.W. Thondapu, V., Hayat, U., Barlis, P., Yap, C.Y., Kuo, P.-H., Wang, Q., Ma, J., Zhu, S.J., Moore, S. & Ooi, A.S.H., Elevated Blood Viscosity and Microrecirculation Resulting From Coronary Stent Malapposition, *J. Biomech. Eng*., **140**, 2018, 051006-1.

[5] Thondapu, V., Tenekecioglu, E., Poon, E.K.W., Collet, C., Torii, R., Bourantas, C.V., Chin, C., Sotomi, Y., Jonker, J., Dijkstra, J., Revalor, E., Gijsen, F., Onuma, Y., Ooi, A., Barlis, P. & Serruys, P.W., Endothelial Shear Stress 5 Years After Implantation of a Coronary Bioresorbable Scaffold, *Eur. Heart J.*, **39**(18), 2018, 1602–1609.

[6] Beier, S., Ormiston, J., Webster, M., Cater, J., Norris, S., Medrano-Gracia, P., Young, A. & Cowan, B., Hemodynamics in Idealized Stented Coronary Arteries: Important Stent Design Considerations, *Ann. Biomed. Eng*., **44**(2), 2016, 315–329.

[7] Foin, N., Guti_errez-Chico, J.L., Nakatani, S., Torii, R., Bourantas, C.V., Sen, S., Nijjer, S., Petraco, R., Kousera, C., Ghione, M., Onuma, Y., Garcia-Garcia, H.M., Francis, D.P., Wong, P., Di Mario, C., Davies, J.E. & Serruys, P.W., Incomplete Stent Apposition Causes High Shear Flow Disturbances and Delay in Neointimal Coverage as a Function of Strut to Wall Detachment Distance: Implications for the Management of Incomplete Stent Apposition, *Circ. Cardiovasc. Interventions*, **7**(2), 2014, 180–189.

[8] Quemada, D., Rheology of Concentrated Disperse Systems—Part III: General Features of the Proposed Non-Newtonian Model. Comparison With Experimental Data, *Rheol. Acta*, **17**(6), 1978. 643–653.

[9] Davies, J.E., Parker, K.H., Francis, D.P., Hughes, A.D. & Mayet, J., What is the Role of the Aorta in Directing Coronary Blood Flow?, *Heart*, **94**(12), 2008 1545–1547.

[10] Tenekecioglu, E., Torii, R., Bourantas, C.V., Al-Lamee, R. & Serruys P.W., Non-Newtonian pulsatile shear stress assessment: a method to differentiate bioresorbable scaffold platforms, *Eur. Heart J.*, **38**(33), 2017, 2570.

[11] Malek, A.M., Alper, S.L. & Izumo, S., Hemodynamic Shear Stress and Its Role in Atherosclerosis, *J. Am. Med. Assoc.*, 282(21), 1999, 2035–2042.

[12] Virchow, R., As Based Upon Physiological and Pathological Histology, *Nutr. Rev.*, **47**(1), 1989, 23–25.

[13] Davies, J.E., Whinnett, Z.I., Francis, D.P., Manisty, C.H., Aguado-Sierra, J.,Willson, K., Foale, R. A., Malik, I.S., Hughes, A.D., Parker, K.H. & Mayet, J., Evidence of a Dominant Backward-Propagating 'Suction' Wave Responsible for Diastolic Coronary Filling in Humans, Attenuated in Left Ventricular Hypertrophy, *Circulation*, **113**(14), 2006, 1768–1778.

[14] Peacock, J.A., An In Vivo Study of the Onset of Turbulence in the Sinus of Valsalva," *Circ. Res.*, **67**(2), 1990, 448–460.